Received: 28 March 2020 | Revised: 6 May 2020 | Accepted: 17 May 2020

DOI: 10.1002/bio.3883

RESEARCH ARTICLE

LUMINESCENCE The Journal of Biological and Chemical Luminescence WILEY

Design and synthesis of two new terbium and europium complex-based luminescent probes for the selective detection of zinc ions

Abdul Waheed[1] | Safwat Abdel-Azeim[2] | Nisar Ullah[1] | Sulayman A. Oladepo[1]

[1]Chemistry Department, King Fahd University of Petroleum and Minerals, Dhahran, Saudi Arabia

[2]Center of Integrative Petroleum Research, College of Petroleum Engineering and Geosciences (CPG), King Fahd University of Petroleum and Minerals, Dhahran, Saudi Arabia

Correspondence
Nisar Ullah, Chemistry Department, King Fahd University of Petroleum and Minerals. Dhahran, Saudi Arabia.
Email: nullah@kfupm.edu.sa

Funding information
King Fahd University of Petroleum and Minerals, Grant/Award Number: DF181029

Abstract

Zinc plays a key role in many physiological processes and has implications for the environment. Consequently, detection of chelatable zinc ion (Zn^{2+}) has attracted widespread interest from the research community. Lanthanide-based luminescent probes offer particular advantages, such as high water solubility, long luminescence lifetimes and a large Stokes' shift, over common organic dye-based fluorescent sensors. Here, we report the synthesis of terbium and europium complex-based probes, **Tb-1** and **Eu-1**, for sensitive and selective detection of Zn^{2+} in water. These probes featured the incorporation of bis(2-pyridylmethyl)]amine (DPA) receptor for Zn^{2+} chelation and the 1,4,7-tris(carboxymethyl)-1,4,7,10-tetraazacyclododecane (DO3A) ring to chelate lanthanide (Ln^{3+}). **Tb-1** and **Eu-1** displayed high selectivity for Zn^{2+} ions over a wide range of competing ions, with limits of detection of 0.50 ± 0.1 μM and 1.5 ± 0.01 μM, respectively. Density functional theory simulations were in good agreement with experimental observations, displaying high Zn^{2+} selectivity compared with most competing ions. In the competing ions experiments, the luminescence response of **Tb-1** and **Eu-1** was moderately quenched by some ions such as Cu^{2+}, this was linked to the comparable binding abilities of these ions for the receptor of the probe.

KEYWORDS

europium complex, luminescent probe, terbium complex, zinc chemosensor, zinc ions

1 | INTRODUCTION

Zinc is an essential metal that plays some fundamental structural and/or functional roles in the human body.[1] As the second most abundant metal after iron,[2] zinc exists in its Zn^{2+} form in all tissues and fluids. In multicellular organisms, zinc is predominately found inside cells, therefore zinc is involved in structural, catalytic, and regulatory roles at the cellular level.[3] Zinc is considered to be nontoxic, but its deficiency or its excess in the body can be harmful, causing clinical conditions and adverse consequences to human health.[4] For example, in patients with breast cancer, zinc concentrations in serum and hair sample were found to be lower than normal.[5] In addition, due to the modulatory role of zinc in neurotransmission, the pathology of disorders such as Parkinson's disease, epilepsy, Alzheimer's disease and cerebral ischaemia arises from disruption of Zn^{2+} homeostasis.[6] Imbalance of Zn^{2+} in the human body can result in type 1 or type 2 diabetes.[7] Finally, excess zinc in the environment results in decreased microbial activity, which ultimately leads to decreased soil fertility.[8] Zinc is discharged into the environment from industries that make alloys and protecting steel, batteries, and oxide fillers for corrosion.[9]

In the light of the above, it is highly desirable to develop water-soluble chemosensors that could be used to detect Zn^{2+} ions for use in environmental monitoring and biological systems. Such

sensors would enable zinc biochemistry to be deciphered, which, in turn, is crucial for understanding its physiological and pathological roles. However, Zn^{2+} is spectroscopically and magnetically inactive due to its $d^{[10]}$ electron configuration, which makes its detection complicated. Increasing levels of Zn^{2+} in water bodies due to the abundant use of zinc in industry has led to the development of numerous analytical methods for detection of Zn^{2+} including atomic absorption spectroscopy (AAS), inductively coupled plasma mass spectrometry (ICP-MS), X-ray fluorescence (XRF), atomic emission spectroscopy (AES) and electrochemical techniques. Nevertheless, these techniques require expensive instrumentation, have time-consuming procedures and involve laborious sample preparation.[10] In recent years, organic dye-based fluorescent probes due to their high sensitivity and operational simplicity for real-time analysis have gained significant attention for detection and quantification of Zn^{2+} ions . However, these probes have short fluorescence lifetimes, and show interference due to autofluorescence from the biological matrix, undergo photobleaching, and have small Stokes' shifts, all of which may lead to experimental errors caused by excitation and light scattering.[11] In contrast, lanthanide (Ln) complex-based luminescent probes exhibit sharp line-like emission bands and long luminescence lifetimes.[12] Therefore, fast-decaying background signals (scattering or autofluorescence) in the nanosecond range can be discriminated from Ln luminescence (in the microsecond or millisecond range). In addition, Ln complexes generally provide tunable colours, large Stokes' shifts, and high water solubility.[13] Consequently, several Ln-based probes for detection of Zn^{2+} ions have been studied.[14,15]

Parker and colleagues reported 1,4,7,10-tetraazacyclododecane-1,4,7,10-triacetic acid (DOTA) complexes for Tb^{3+} and Eu^{3+}. Upon binding with Zn^{2+}, the luminescence of these complexes increased to 42% and 26%, respectively.[16] However, selective competition of these probes was not studied comprehensively. In another report, Tuck and colleagues documented the synthesis and detection of Zn^{2+} by Tb-5 and Eu-6. These probes, upon complexing with Zn^{2+}, gave luminescence enhancements of 2.1-fold and 3.4-fold, respectively. However, the selectivity performance of these probes turned out to be poor, in particular for Cd^{2+}, Fe^{3+} and Hg^{2+}, and resulted in an increase in basal luminescence of the probes.[17] Despite impressive progress, the existing probes have numerous limitations such as selectivity, sensitivity, the ability to cover large zinc concentration ranges, and optical compatibility with biological samples.[18,19]

Stability of the Ln complex in solution is vital to suppress deactivation of Ln^{3+} excited states nonradiatively and to avoid the risk of toxicity resulting from free Ln^{3+}. Similarly, the denticity or coordination number of the chelating ligand is important to protect the metal centre from solvent coordination. A low coordination number for the chelating ligand would allow coordination of solvent molecules, such as water, which in turn would lead to non-radiative deactivation of excited Ln^{3+} by nonradiative vibrational energy transfer to high-frequency O–H oscillators.[20] DOTA and 1,4,7-tris(carboxymethyl)-1,4,7,10-tetraazacyclododecane (DO3A) are the most frequently used chelating ligands as they form Ln complexes with enhanced kinetic inertness and high thermodynamic stability.[21–23]

In light of the above, we synthesized luminescent Ln-based probes **Tb-1** and **Eu-1** (Figure 1) and evaluated them for selective detection of Zn^{2+} ions in water. The design of these probes was based on incorporating bis(2-pyridylmethyl)]amine (DPA) receptor for Zn^{2+} chelation, and the DO3A ring to chelate Ln^{3+}. The receptor and fluorescence emission resource (DO3A ring) were connected via a phenyl chromophore, which contained both $\pi-\pi^*$ and $n-\pi^*$ transitions. The design of these probes was expected to allow six-membered metal–ligand complexes in the amide tautomer form (Figure 1). According to the ligand design concepts,[24,25] six-membered coordination rings would increase selectivity for smaller metal ions such as Zn^{2+}, over larger metal ions such as Cd^{2+}. This in turn could result in high affinity and selectivity for Zn^{2+} in a competitive medium over several other biologically or environmentally important cations.

2 | EXPERIMENTAL

2.1 | Materials and instrumentation

Unless otherwise noted, reagents and solvents were used as received, without further purification, from commercial suppliers. ^{1}H-NMR and ^{13}C-NMR spectra were obtained on a JEOL spectrometer (JNM-LA 500 MHz, JEOL USA Inc.), whereas infrared spectra were obtained on a Perkin-Elmer spectrometer (16F PC FTIR, Perkin-Elmer Inc., USA). HRMS (ESI) data were obtained on an ABSciex instrument (Germany) (50 kV) and XPS analysis was performed on a Thermos Scientific Escalab 250Xi spectrometer, equipped with an Al Kα (1486.6 eV) monochromated X-ray source with 5×10^{-10} mbar base pressure in

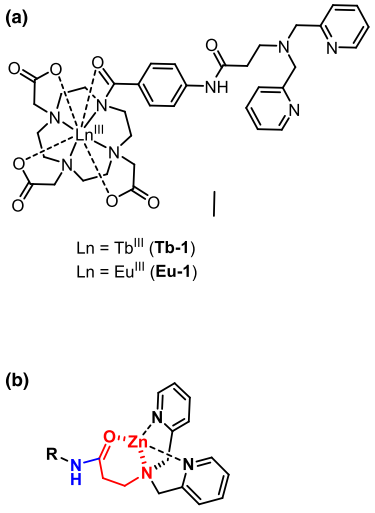

FIGURE 1 (a) Chemical structures of **Tb-1** and **Eu-1**. (b) Expected high affinity and selectivity for Zn^{2+}

the analysis chamber. A low energy electron flood gun was used for surface charge compensation. Spectrometer energy was calibrated by fixing Cu 2p3/2, Ag 3d5/2 and Au 4f7/2 peaks at binding energies of 932.6, 368.2 and 83.9 eV, respectively. Density functional theory (DFT) calculation details along with output files are given in Supporting Information (Computational Details). Luminescence studies were performed on a fluorescence spectrophotometer (Edinburgh). Luminescence data were recorded in aqueous solution at pH 7, using 20 mM HEPES buffer. Similarly, absorption spectra for **Tb-1** and **Eu-1** (Figure S1) were recorded on a GENESYS 10S UV–vis spectrophotometer.

2.2 | Synthesis of compounds

2.2.1 | Synthesis of ethyl 3-(bis (pyridin-2-ylmethyl) amino)propanoate (3)

K_2CO_3 (5.41 g, 39.1 mmol) was added to a solution of ethyl 3-aminopropionate **2** (1.0 g, 6.53 mmol) in anhydrous acetonitrile (80 ml) at room temperature and stirred for 15 min, then 2-(bromomethyl)pyridine hydrobromide (4.12 g, 16.2 mmol) was added and the mixture was refluxed for 6 h. After completion of the reaction (TLC analysis), the solvent was removed under reduced pressure. A dark brown oily residue was resolved using a silica column, and eluting with hexane-ethyl acetate (50:50 to 10:90) to produce compound **3** as a light brown oil (2.2 g, 86%). IR (KBr): 3009, 2953, 2816, 1729, 1567, 1435, 1316, 1047, 763 cm^{-1}. ^{1}H-NMR (500 MHz, $CDCl_3$): δ 8.39 (2H, d, *J* = 4.60 Hz, Ar-H), 7.53 (2H, t, *J* = 7.33 Hz, Ar-H), 7.38 (2H, d, *J* = 7.63 Hz, Ar-H), 7.02 (2H, t, *J* = 6.10 Hz, Ar-H), 3.98 (2H, q, *J* = 7.02 Hz, CH_2), 3.74 (4H, s, 2 x CH_2), 2.84 (2H, t, *J* = 6.86 Hz, CH_2), 2.45 (2H, t, *J* = 7.0 Hz, CH_2), 1.09 (3H, t, *J* = 7.0 Hz, CH_3). ^{13}C-NMR (125.7 MHz, $CDCl_3$): δ 171.98, 159.03, 148.56, 135.97, 122.55, 121.62, 59.89, 59.73, 49.55, 32.35, 13.80. Anal. Calcd for $C_{17}H_{21}N_3O_2$: C, 68.20, H, 7.07, N, 14.04. Found: C, 68.10, H, 7.14, N, 13.95.

2.2.2 | Synthesis of 3-(bis (pyridin-2-ylmethyl)amino) propanoic acid (4)

1 M sodium hydroxide (13 ml, 13.0 mmol) was added to a solution of ester **3** (0.75 g, 2.52 mmol) in a mixture of methanol and water (1:2, 15 ml) at room temperature and the reaction was stirred overnight; solvents were evaporated under reduced pressure. Column chromatography of the brown oily material, followed by elution with methanol–chloroform (5:95 to 10:90) yielded the desired **4** as a light brown oil (0.53 g, 78%). IR (KBr): 3365, 3001, 2948, 2801, 1714, 1560, 1430, 1292, 1027, 761 cm^{-1}. ^{1}H-NMR (500 MHz, CD_3OD): δ (ppm) 8.39 (2H, d, *J* = 4.58, Ar-H), 7.76 (2H, t, *J* = 7.62, Ar-H), 7.58 (2H, d, *J* = 7.63 Hz, Ar-H), 7.24 (2H, t, *J* = 5.80 Hz, Ar-H), 3.78 (4H, s, 2 x CH_2), 2.85 (2H, t, *J* = 7.32 Hz, CH_2), 2.43 (2H, t, *J* = 7.36 Hz, CH_2). ^{13}C-NMR (125.7 MHz, CD_3OD): δ 181.19, 160.28, 149.20, 138.64, 124.83, 123.64, 60.6, 52.9, 36.6. Anal. Calcd for $C_{17}H_{21}N_3O_2$: C, 66.40, H, 6.32, N, 15.49. Found: C, 66.28, H, 6.45, N, 15.57.

2.2.3 | Synthesis of tert-butyl 2,2′,2″-(10-(4-nitrobenzoyl)-1,4,7,10-tetraazacyclododecane-1,4,7-triyl)triacetate (6)

Et_3N (1.08 ml, 7.80 mmol) was added to a solution of DO3AtBu amine **5** (1.00 g, 1.94 mmol) in CH_2Cl_2 (15 ml) at 0°C under a nitrogen atmosphere. This mixture was then added dropwise to an already cold solution of 4-nitrobenzoyl chloride (0.72 g, 3.89 mmol) in THF (15 ml) at 0°C. The reaction mixture was stirred overnight at room temperature. After completion of the reaction (TLC analysis), solvents were evaporated under reduced pressure and the residue dissolved in CH_2Cl_2 (20 ml) and then washed with water (3 × 10 ml). The organic layer was dried over Na_2SO_4 and evaporated under vacuum. Column chromatography on silica column, followed by elution with methanol–dichloromethane (0:100 to 5:100) gave compound **6** as a yellow oil (1.18 g, 92%). Spectroscopic data matched previously known materials.[26]

2.2.4 | Synthesis of tert-butyl 2,2′,2″-(10-(4-aminobenzoyl)-1,4,7,10-tetraazacyclododecane-1,4,7-triyl)triacetate (7)

Reduced iron powder (0.46 g, 8.2 mmol), NH_4Cl (0.30 g, 5.6 mmol) and glacial acetic acid (8.0 ml) were added to a solution of compound **6** (1.0 g, 1.58 mmol) in a mixture of EtOH and H_2O (2.5:1, 60 ml) and the suspension was sonicated at 50°C for 8 h. After completion of the reaction (TLC analysis), the solid residue was filtered off, and washed with $CHCl_3$ (10 ml). The filtrate was added to $CHCl_3$ (20 ml) and washed with 2 M KOH (3 × 30 ml). The organic layer was dried over Na_2SO_4 and evaporated under reduced pressure. The crude residue was passed through a plug of a silica column to produce compound **7** as a yellow oil (0.68 g, 71%). Spectroscopic data matched previously known materials.[26]

2.2.5 | Synthesis of tert-butyl 2,2′,2″-(10-(4-(3-(bis (pyridin-2-ylmethyl)amino)propanamido)benzoyl)-1,4,7,10-tetraazacyclododecane-1,4,7-triyl)triacetate (8)

HOBT (0.04 g, 0.29 mmol) and Et_3N (0.13 ml, 0.94 mmol) were added sequentially to a solution of **4** (0.07 g, 0.26 mmol) in DMF (8 ml) and the mixture was stirred at 0°C for 30 min. Next, a solution of **7** (0.15 g, 0.23 mmol) in DMF (2 ml) and EDCI (0.06 g, 0.31 mmol) were added to the reaction and stirring was continued for 48 h at room temperature. Upon completion of the reaction (TLC analysis), H_2O (15 ml) was added and the product extracted with ethyl acetate (3 × 20 ml). The organic layer was washed with brine (3 × 10 ml), dried

over Na_2SO_4, and evaporated under reduced pressure. Column chromatography of the brown oily material, followed by elution with methanol–chloroform (0:100 to 10:100) gave the product as a light brown oil (0.14 g, 71%). IR (KBr): 3471, 3006, 2960, 2825, 1751, 1469, 1631, 1470, 1122, 923, 840, 752 cm^{-1}. ^{1}H-NMR (500 MHz, $CDCl_3$): δ 10.93 (1H, s, broad), 8.42 (2H, d, *J* = 5.1 Hz, Ar-H), 7.75 (1H, d, *J* = 7.1 Hz, Ar-H), 7.50 (3H, d, *J* = 7.32 Hz, Ar-H), 7.22 (3H, t, *J* = 7.93 Hz, Ar-H), 7.02–7.07 (3H, br. M, Ar-H), 3.82–3.2.55 (30H, m), 1.38–1.34 (27H, m). ^{13}C-NMR (125.7 MHz, $CDCl_3$): δ 170.79, 170.70, 157.75, 149.88, 149.34, 149.11, 149.07, 136.80, 136.72, 127.43, 123.49, 119.76, 59.73, 53.02, 51.98, 51.22, 50.49, 50.05, 34.40, 28.20, 28.14. Anal. Calcd for $C_{48}H_{70}N_8O_8$: C, 64.99, H, 7.95, N, 12.63. Found: C, 64.58, H, 8.05, N, 12.38.

2.2.6 | (2,2′,2″-(10-(4-(3-(bis (pyridin-2-ylmethyl) amino)propanamido)benzoyl)-1,4,7,10 tetraazacyclododecane-1,4,7-triyl)triacetic acid) (*9*)

Compound **8** (0.1 g, 0.11 mmol) was added to an ice-cold solution of mixture of TFA (3 ml) and H_2O (1 ml) and the reaction mixture was stirred for 72 h at 60°C. After completion of the reaction (TLC analysis), the volatiles were removed under reduced pressure and then co-concentrated with methanol (3 × 3 ml). Titration with diethyl ether produced a trifluoroacetic acid salt of the desired **9** as a light brown solid [0.06 g, 49%, based on tris(trifluoroacetic acid) salt]. IR (KBr): 3436, 3096, 2925, 2852, 1737, 1631, 1597, 1473, 1048, 846, 763 cm^{-1}. ^{1}H-NMR (500 MHz, D_2O): δ 8.52 (2H, d, *J* = 4.90 Hz, Ar-H), 8.22 (2H, t, *J* = 8.24 Hz, Ar-H), 7.80–7-7.67 (4H, m, Ar-H), 7.40–7.26 (2H, m, Ar-H), 4.20 (4H, s), 3.57–2.52 (26H, m). ^{13}C-NMR (125.7 MHz, D_2O): δ 175.18, 165.60, 165.32, 155.27, 151.82, 147.65, 147.25, 145.57, 145.39, 128.22, 123.11, 58.94, 53.60, 53.23, 52.97, 52.81, 52.66, 52.56, 36.16. HRMS (ESI^+): calcd for $C_{36}H_{46}N_8O_8$ $[M + H]^+$: 719.3439. Found: 719.3517 (Figure S4).

2.2.7 | Synthesis of Tb-1 and Eu-1

Compound **9** (0.041 g, 0.04 mmol) was dissolved in H_2O (0.5 ml) and pH was adjusted to 8 with 1 M NaOH (aq.). Next, a solution of Ln $(CF_3SO_3)_3$ (0.09 mmol) in H_2O (0.5 ml) was added dropwise and the mixture was heated at 70°C for 72 h. The pH was monitored periodically and maintained at 8 with 1 M NaOH (aq.) as needed. Upon completion of the reaction, the precipitated $Ln(OH)_3$ was removed by centrifugation. The filtrate was lyophilized to yield the title compounds as white solids, which were then dissolved in a mixture of methanol–ethanol (2:1) and excess salts were separated by centrifugation to produce **Tb-1** (0.021 g, 60%) and **Eu-1** (0.019 g, 55%) as a white solid. **Tb-1**: HRMS (ESI^+): calcd for $C_{36}H_{43}N_8O_8Tb$ $[M + H]^+$: 874.2457, found: 875.2516. **Eu-1**: HRMS (ESI^+): calcd for $C_{36}H_{43}EuN_8O_8$ $[M + H]^+$: 868.2416. Found: 869.2472 (Figures S5 and S6).

3 | RESULTS AND DISCUSSION

3.1 | Design and synthesis of Tb-1 and Eu-1

Design of luminescent lanthanide-based probes was based on covalently attaching an appropriate antenna, phenyl chromophore that contained both π– π* and n– π* transitions, and incorporation of a DO3A ligand to chelate the lanthanide ion. DO3A could provide thermodynamic stability and kinetic inertness to the lanthanide chelate.[27] The design of these probes would permit six-membered metal–ligand complexes in the imidic acid tautomer form (Figure 1), which in turn would allow enhanced selectivity for Zn^{2+} over larger metal ions such as Cd^{2+}. The synthesis of luminescent probes **Tb-1** and **Eu-1** necessitated the preparation of intermediate **4**, which in turn was synthesized by alkylation of ethyl 3-aminopropanoate **2** with 2-(bromomethyl)pyridine followed by hydrolysis of the ester function under basic conditions (Scheme 1).

Similarly, synthesis of the DO3A-based ligand **9** was accomplished as depicted in Scheme 2. Acylation of DO3A-tris-tert-butyl ester **5** with 4-nitrobenzoyl chloride gave compound **6**, which was transformed to intermediate **7** by reducing the nitro function of the former with Fe in acetic acid. Similarly, amidation of intermediate **7** with acid **4** under standard conditions allowed access to intermediate **8**, which was then transformed to the desired ligand **9** by the action of trifluoroacetic acid in water. Finally, the reaction of ligand **9** with $Tb(OTf)_3$ and $Eu(OTf)_3$, respectively, led to the synthesis of the desired **Tb-1** and **Eu-1** in high yields (Scheme 2).

3.2 | Characterization and luminescence properties of Tb-1

The absorption maximum (λ_{max}) of **Tb-1** was found to be between 225 nm and 275 nm (Figure S1). Figure 2 represents the steady-state luminescence emission of **Tb-1** in the absence or presence of Zn^{2+} ions. It is evident that the neat **Tb-1** complex is weakly luminescent. However, upon addition of Zn^{2+} ions and increasing the concentration from 0.0 to 2.0 equivalents, the luminescence intensity of **Tb-1** was enhanced to almost five-fold. These results indicated that binding of

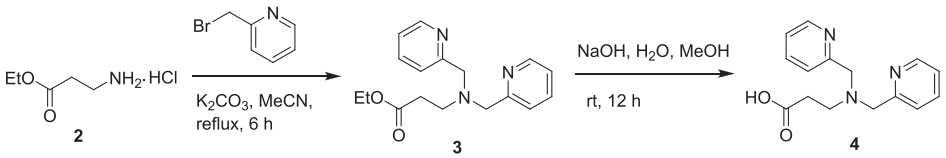

SCHEME 1 Synthesis of intermediate **4**

SCHEME 2 Synthesis of **Tb-1** and **Eu-1**

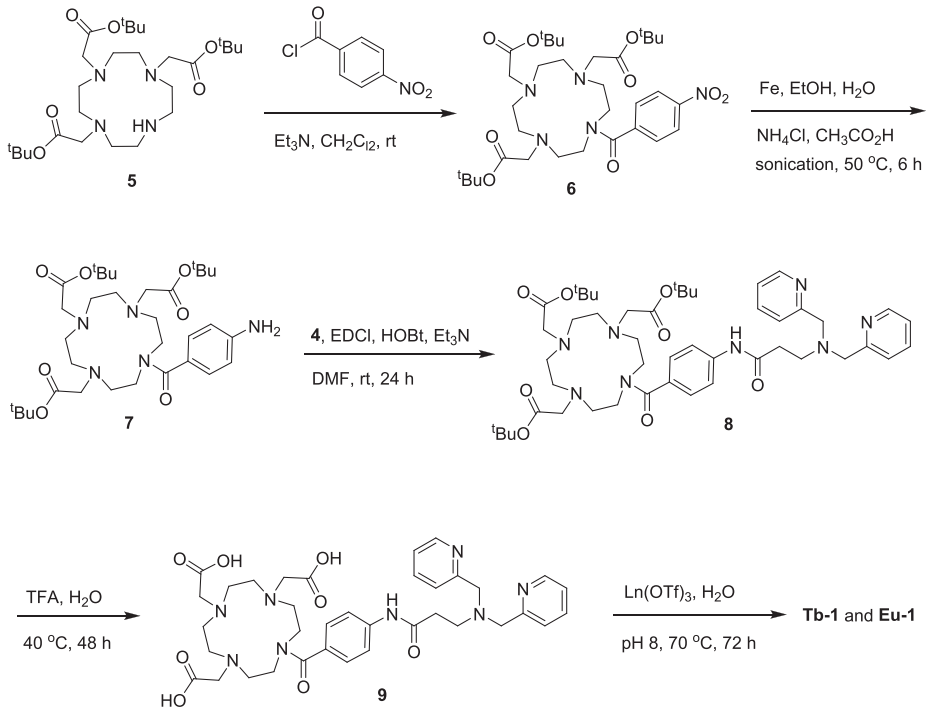

the receptor (DPA) to Zn^{2+} led to inhibition of the photoinduced electron transfer (PeT) process, which in turn modulated the 'off–on' luminescence behaviour of the **Tb-1** complex, therefore affording a distinct signal for the luminescence sensing of Zn^{2+}. When the receptor is in an unbound state ('off-state'), the electron pair in the highest occupied molecular orbital (HOMO) of the tertiary amine nitrogen lies over the S_0 ground state of the antenna. On photoexcitation of the antenna to the S_1 state, PeT from the receptor to the unpaired electron in the S_0 ground state of the antenna occurred. PeT not only enhanced the nonradiative decay of the photoexcited antenna but also reduced its sensitizing efficiency, which in turn resulted in reduced Tb^{3+} luminescence. Upon binding with Zn^{2+}, the lone-pair electrons of the receptor became engaged ('on-state'), which lowered its HOMO to lower than the S_0 ground state of the antenna. This, in turn, inhibited the PeT process and reclaimed the sensitizing ability of the antenna that led to enhanced Tb^{3+} luminescence.[17,28,29] It is pertinent to mention that the luminescence pattern for **Tb-1** showed four distinctive intensity bands in the luminescence emission spectra, with maxima at 489, 548, 586 and 622 nm. These bands were associated with the transitions from the $^5D_4$ excited state of terbium to the $^7F_6$, $^7F_5$, $^7F_4$, and $^7F_3$ ground states.[30] The band at 548 nm was used for subsequent analysis.

Limit of detection (LOD) was calculated using a IUPAC method.[31] By applying the above method, LOD was found to be 0.50 ± 0.1 μM for **Tb-1.** To investigate the selectivity of the **Tb-1** for Zn^{2+} over the various metal ions, the effect of addition of various metal ions on luminescence of **Tb-1** was investigated by adding 1.0 equivalent of each metal cation (Figure 3). The effect of various metal ions on the luminescence was investigated at pH 7.0 (20 mmol HEPES). Most metal cations did not show any increase in basal luminescence for **Tb-1**, instead intensity of luminescence decreased, except for $Na^{1+}$and Ba^{2+} for which the luminescence intensity of **Tb-1** slightly increased (Figure 3). Moreover, Cu^{2+} and Fe^{3+} completely quenched the luminescence of **Tb-1** (Figure 3). However, the addition of 1 equivalent of Zn^{2+} to the solutions of these metal ions produced a marked luminescence response, which suggested that **Tb-1** is a selective chemosensor for Zn^{2+}.

3.3 | Characterization and luminescence properties of Eu-1

The absorption spectrum for **Eu-1** was quite similar to that of **Tb-1** with λ_{max} in the region 225–275 nm. The luminescence pattern for **Eu-1** showed four distinctive bands at 579, 605, 635 and 690 nm, which correspond to relaxation from $^5D_0$ to $^7F_0$, $^7F_1$ and $^7F_2$ and $^7F_3$ ground states, respectively.[30,32] Luminescence intensity of **Eu-1** was found to increase two-fold with the gradual increase in Zn^{2+} from 0.0 to 2.0 equivalents (Figure 4). Moreover, LOD for **Eu-1** was determined using the above method and was found to be 1.5 ± 0.01 μM.

To determine the effect of various ions on luminescence of **Eu-1**, various ions were added to **Eu-1** at a metal cation molar ratio of 1:1 (Figure 5). The response of Zn^{2+} was quite vivid and obvious compared with the response of other metal cations, making the sensor quite selective for the target metal ion, i.e. Zn^{2+}. However, most ions caused a decrease in the basal luminescence of the **Eu-1**, especially copper and iron ions. In the competing ions experiment, the response of the sensor was least affected by Na^+ and Ba^{2+}, while Cu^{2+} and Fe^{3+} resulted in quenching of the **Eu-1** response.

XPS analysis of **Tb-1** and **Eu-1** was performed to confirm the chemical composition of these complexes (Figure 6). A line shape

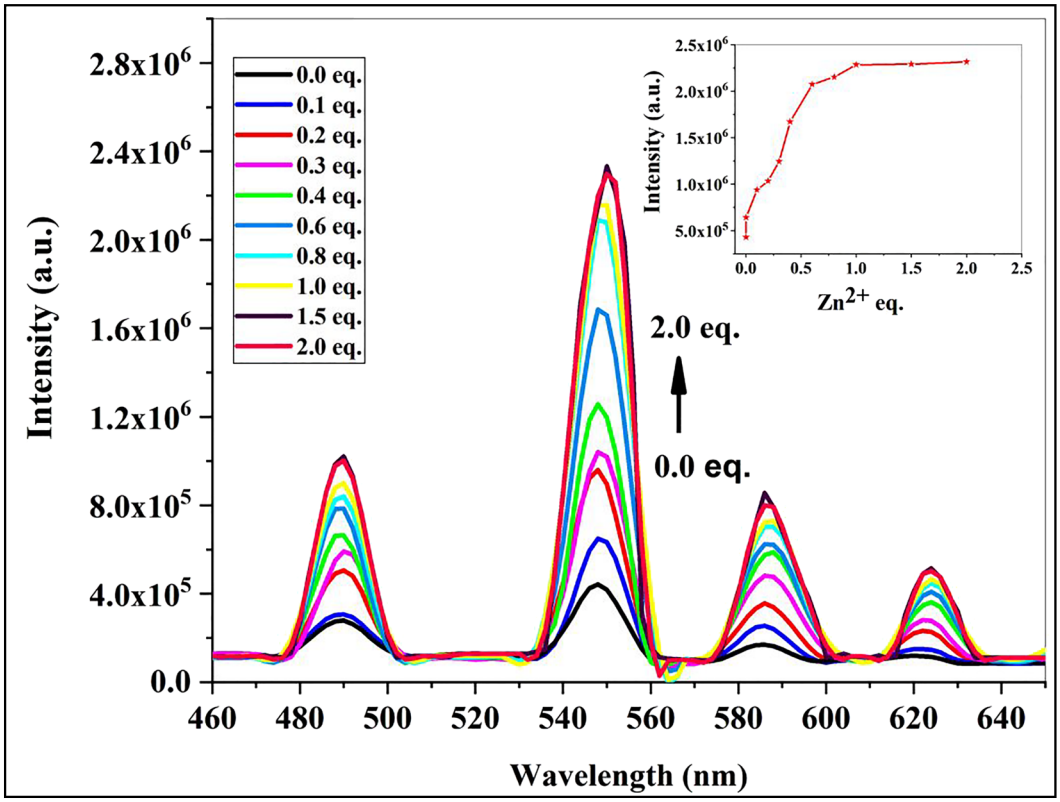

FIGURE 2 Response of **Tb-1** to increasing concentrations of Zn^{2+} (λ_{ex} = 265 nm, 1 cm quartz cell, pH 7.0, 20 mM HEPES buffer). Inset shows changes in the luminescence intensity measured at 548 nm

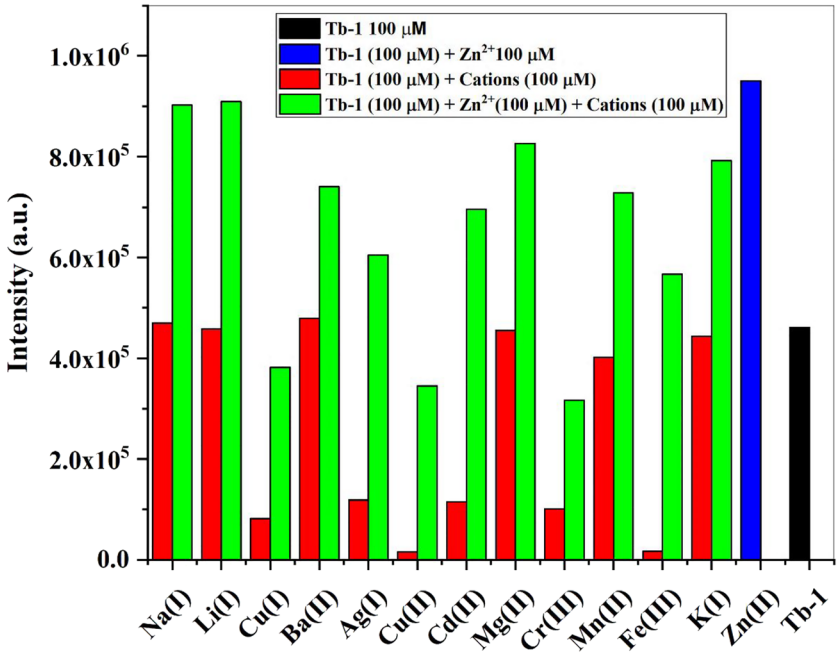

FIGURE 3 Changes in the luminescence of 100 μM **Tb-1** (λ_{ex} = 265 nm, λ_{em} = 548 nm, 1 cm quartz cell, pH 7.0, 20 mM HEPES buffer) upon addition of 1.0 equivalent of different metal ions in the presence or absence of Zn^{2+}

analysis with Gaussian fitting was applied to draw plots from the XPS spectra. A wide scan survey analysis of **Tb-1** (Figure 6a) and **Eu-1** (Figure 6b) exhibited peaks at 1240 eV and 1140 eV due to binding energies by Tb^{3+} ($3d_{5/2}$) and Eu^{3+} ($5d_{3/2}$), respectively. In addition, high-resolution XPS analysis showed multiplet structures in Tb^{3+} ($3d_{5/2}$) (Figure S2a)[32] and Eu^{3+} ($5d_{3/2}$) (Figure S2b) regions.[33] A multiplet structure is indicative of the high binding energies of Tb^{3+} and Eu^{3+} with the ligand. Detailed XPS analysis of **Tb-1** and **Eu-1** for the binding energies of nitrogen, oxygen and carbon is given (Figure S3).

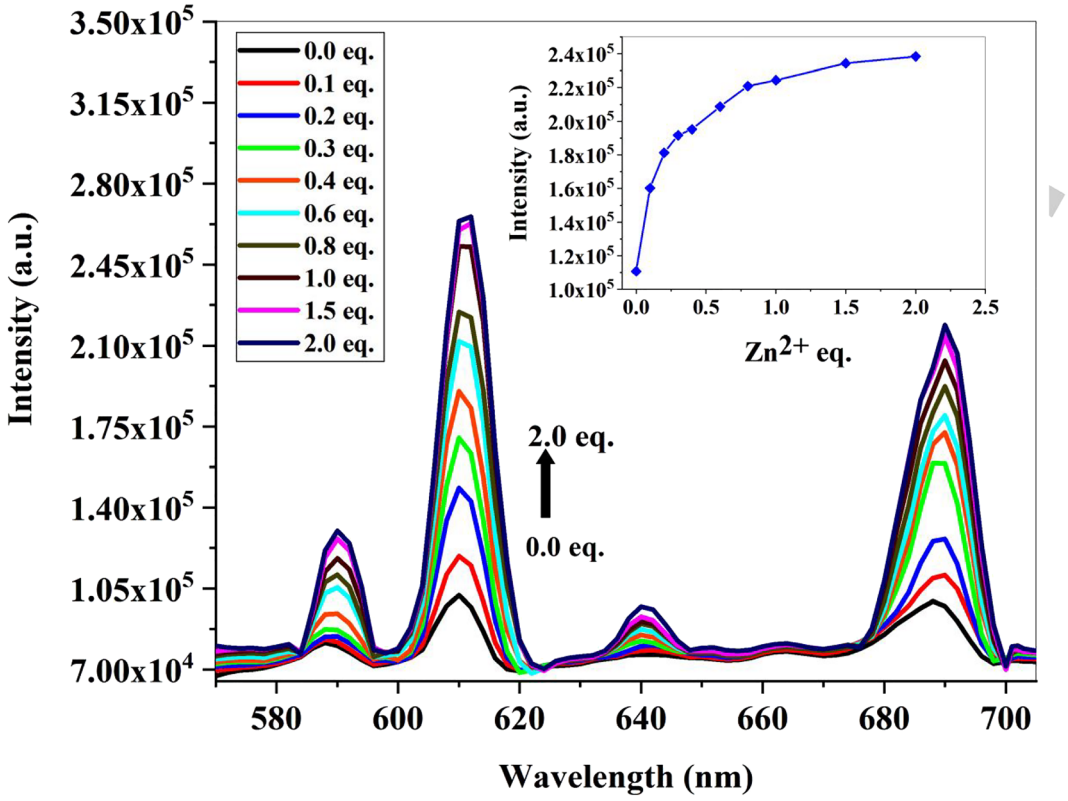

FIGURE 4 Response of **Eu-1** to increasing concentrations of Zn^{2+} (λ_{ex} = 285 nm, 1 cm quartz cell, pH 7.0, 20 mM HEPES buffer). Inset shows changes in the luminescence intensity measured at 610 nm

FIGURE 5 Changes in luminescence of 200 μM **Eu-1** (λ_{ex} = 280 nm, λ_{em} = 610 nm, 1 cm quartz cell, pH 7.0, 20 mM HEPES buffer) upon addition of 1 equivalent of different metal ions in the presence or absence of Zn^{2+}

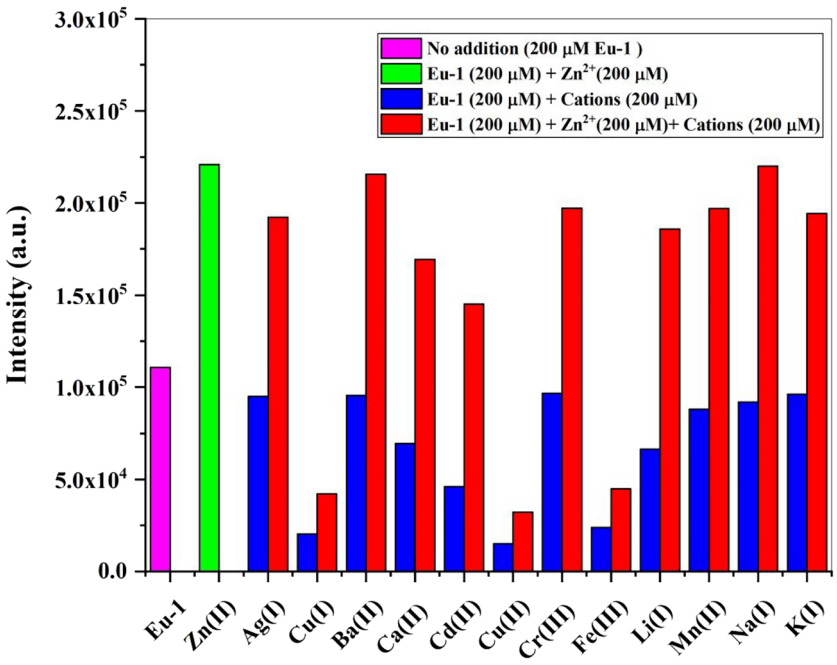

3.4 | Computational studies

DFT simulations were employed to explain the effect of various ions on the luminescence of **Tb-1** and **Eu-1**. For ease and simplicity, DFT calculations were limited to the metal–receptor part of the sensors only, as the lanthanide part is thermodynamically and kinetically stable and not involved in metal binding. For this purpose, representative ions such as Na^+, Zn^{2+}, Cu^+ and Cu^{2+} were selected. It is pertinent to mention that when metal solvation free energies were calculated, the solvation model based on density (SMD) did not reproduce the

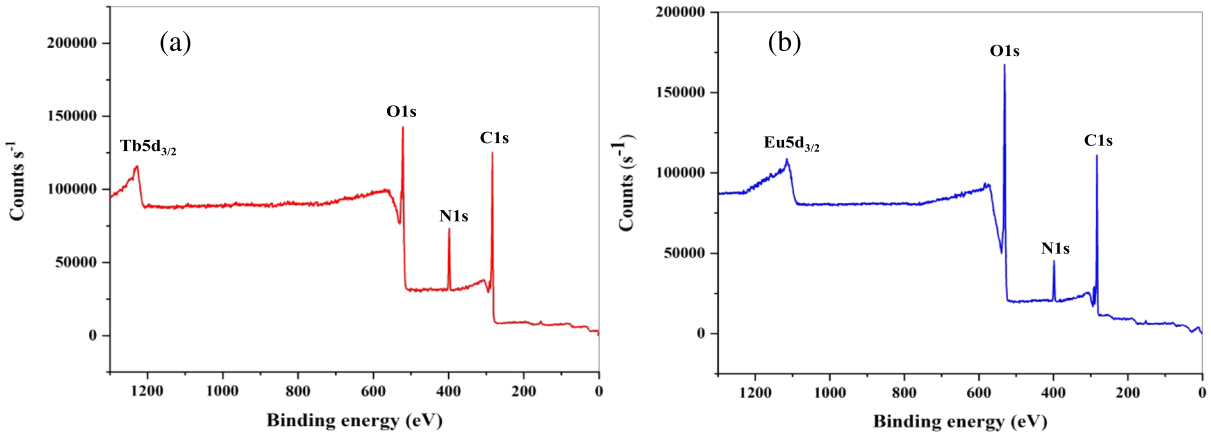

FIGURE 6 X-ray photoelectron spectroscopy (XPS) analysis of (a) **Tb-1** and (b) **Eu-1** indicating peaks in the region of Tb^{3+} and Eu^{3+}

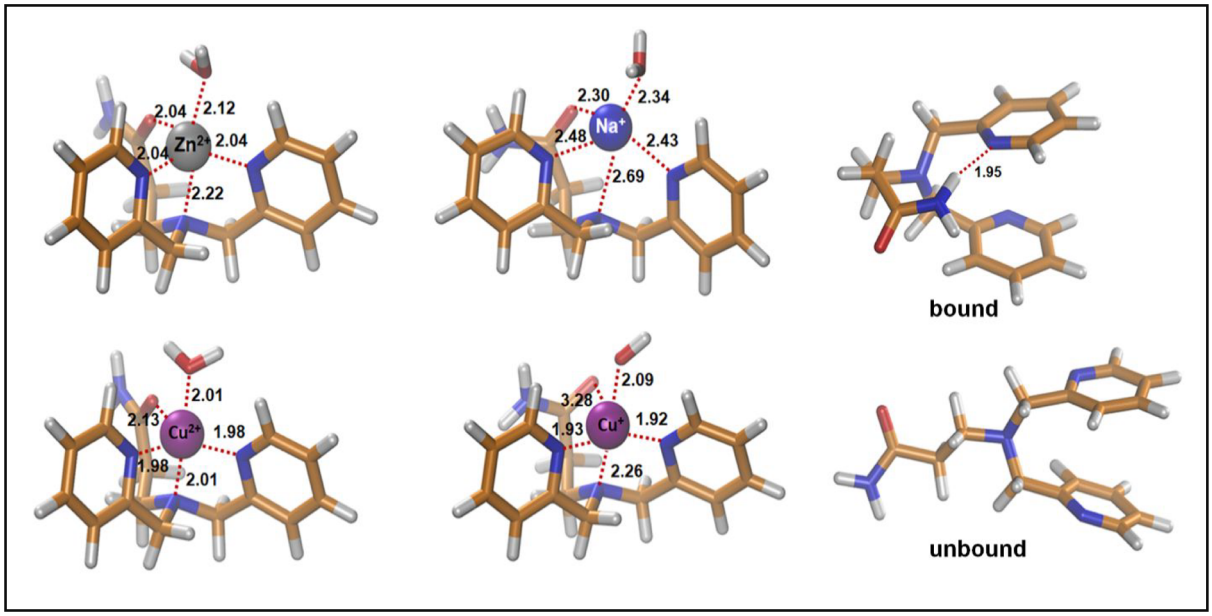

FIGURE 7 Optimized structures of metal–receptor complexes for Zn^{2+}, Na^{+}, Cu^{+}, and Cu^{2+} ions are shown as sticks and ions as balls. Coordination distances are reported in Å. Two unbound states of the antenna molecule are also shown

experimental values. Therefore, to get reliable metal binding free energies, atomic radii were optimized in the continuum solvent model (CSM) by minimizing the difference between the calculated solvation energy and the experimental counterpart (Table S1). After, minimizing the error of the metal solvation free energies, optimized parameters were then used to calculate the solvation free energies of the metal complexes.[34] The optimized structures (Figure 7) adopted a distorted trigonal bipyramid geometry, except for Cu^{+}, which assumed a square planar structure. The average metal–ligand distance among Zn^{2+}, Cu^{+} or Cu^{2+} did not change significantly (2.10 Å for Zn^{2+}, 2.00 Å for Cu^{2+}, and 2.01 Å for Cu^{+}). However, Na^{+} (2.45 Å) displayed a large metal–ligand distance due to differences in its ionic radii. The Cu^{+} complex (square planar) in the Cu^{2+} electronic state (charge = 2, spin = doublet) was also re-optimized, which resulted in a trigonal bipyramid geometry. This indicates that trigonal and square planar are intrinsic geometries of Cu^{2+} and Cu^{+} complexes, respectively, and not due to the initial structures.

TABLE 1 Metal binding free energies of our considered metals to the receptor part of the Ln complex. Total free energy, gas phase, and solvation (including ligand strain energy with 1.89 kcal/mol as a correction added to the free energy to adjust the value from 1.0 atm to the 1.0 M standard) are reported in kcal/mol

Metal ions	ΔE_{gas}	$\Delta E_{Sol.}$	ΔE_{Total}
Na(I)	−105.1	87.1	−18.0
Zn(II)	−414.2	350.1	−64.1
Cu(II)	−439.1	364.7	−74.4
Cu(I)	−154.9	117.4	−37.5

The metal binding free energies trend (Table 1 and Figure 8) suggested favourable binding for the selected metal ions to the receptors of **Tb-1** and **Eu-1**. It is worth mentioning that the current study

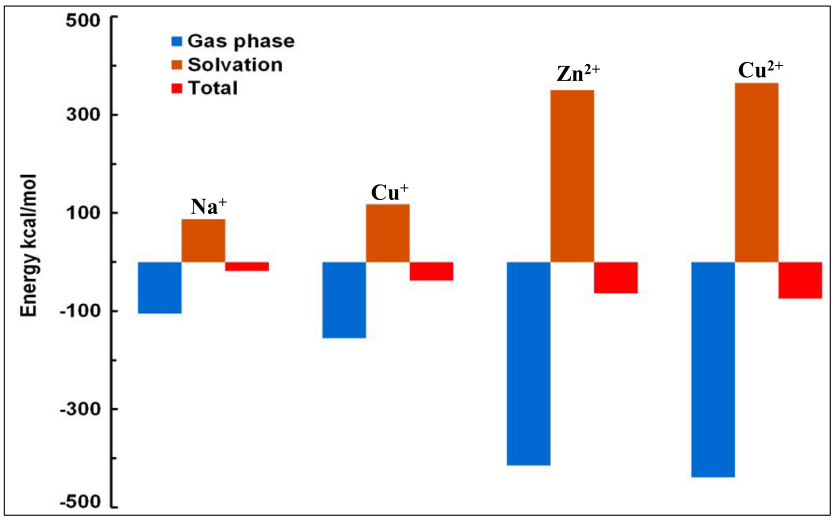

FIGURE 8 Total receptor–metal binding free energies for Na(I), Cu(I), Cu(II), and Zn(II) ions, gas phase, and solvation contributions are shown

was directed towards relative binding free energy rather than absolute binding free energy. In fact, metal–ligand binding events possess a complex potential energy surface, which could not be deduced by single configuration calculations. However, the driving force of metal–receptor binding turned out to be electrostatic interactions and dehydration free energies, which allowed preference towards various metal bindings to the receptor. Despite favourable binding in the gas phase, which is mainly electrostatic in nature, metal dehydration free energies are the main barrier for metal binding. Furthermore, ligand strain energy (taken as the energy difference between bound and unbound receptor structures), was found to be 7.5 cal/mol, with changes less than 0.2 kcal/mol among all the metal ions. In addition, the vibrational correction did not exceed 0.7 kcal/mol. Based on the relative binding energies (Table 1), the DPA receptor exhibited selectivity toward Zn^{2+} over Na^{+} and Cu^{+} ions.

Cu^{2+} binding was found to be comparable with that of Zn^{2+} due to their similar ionic radii. Significant charge transfer from the receptor to the metal, as for Cu^{2+}, is the origin of such a strong interaction. Mullikan charge analysis of the two complexes revealed charges of 0.36e and 0.03e for Zn^{2+} and Cu^{2+}, respectively (see Table S2). Higher charge transfer from ligand to Cu^{2+} was presumably due to unfilled d orbitals.[35] Nevertheless, the higher selectivity for Zn^{2+} predicted by DFT simulation was in complete agreement with the experimental observation for the competing ions experiments (Figures 3 and 5).

Tb-1, and **Eu-1** exhibited high selectivity for Zn^{2+} over most of the competing ions in the competition experiment. However, partial luminescence quenching was observed by addition of some competing ions such as Cu^{2+} and Fe^{3+}, and was attributed to their competing binding ability for the receptor.

4 | CONCLUSION

In summary, we successfully synthesized excellent and promising sensors **Tb-1** and **Eu-1,** which are highly selective for detection of target Zn^{2+} at nM concentrations. The sensors have salient features such as presence of DPA and amide linkage for binding the target metal i.e. Zn^{2+}. The sensors had a cyclene analogue, which possessed carboxylic groups, a perfect ligand for binding Tb^{3+} and Eu^{3+}. Both sensors did not show an appreciable increase in basal luminescence when applied to other competing ions including Na^{+}, K^{+}, Ca^{2+}, Mg^{2+} and Ba^{2+}. DFT simulations predicted that the newly synthetized sensors displayed high Zn^{2+} selectivity over other competing ions. Moreover, theoretical calculations also suggested the participation of carbonyl function along with the three nitrogen atoms of DPA in binding to Zn^{2+}, leading to the formation of a six-membered ring in coordination with Zn^{2+} having a slightly distorted trigonal bipyramidal geometry. Therefore, sensors can be easily utilized for tracking Zn^{2+} in aqueous medium with high sensitivity and very low limits of detection.

ACKNOWLEDGEMENTS

Financial support from the King Fahd University of Petroleum & Minerals project # DF181029 is gratefully acknowledged.

ORCID

Abdul Waheed https://orcid.org/0000-0002-5603-5507
Nisar Ullah https://orcid.org/0000-0002-8172-2771

REFERENCES

[1] Y. Liu, Y. Li, Q. Feng, N. Li, K. Li, H. Hou, B. Zhang, *Luminescence* **2018**, *33*, 29.
[2] M. Stefanidou, C. Maravelias, A. Dona, C. Spiliopoulou, *Arch. Toxicol.* **2006**, *80*, 1.
[3] M. Isaac, A. Pallier, F. Szeremeta, P. A. Bayle, L. Barantin, C. S. Bonnet, O. Sénèque, *Chem. Commun.* **2018**, *54*, 7350.
[4] N. Roohani, R. Hurrell, R. Kelishadi, R. Schulin, *J. Res. Med. Sci.* **2013**, *18*, 144.
[5] L. Jouybari, F. Kiani, A. Akbari, A. Sanagoo, F. Sayehmiri, J. Aaseth, M. S. Chartrand, K. Sayehmiri, S. Chirumbolo, G. Bjørklund, *J. Trace Elem. Med. Biol.* **2019**, *56*, 90.
[6] S. Erdemir, S. Malkondu, O. Kocyigit, *Luminescence* **2019**, *34*, 106.
[7] A. Fukunaka, Y. Fujitani, *Int. J. Mol. Sci.* **2018**, *19*, 476.
[8] A. Łukowski, D. Dec, *Environ. Monit. Assess.* **2018**, *190*, 1.

[9] V. Caramia, B. Bozzini, *Mater. Renew. Sustain. Energy* **2014**, *3*, 1.
[10] M. V. Karmegam, S. Karuppannan, D. B. Christopher Leslee, S. Subramanian, S. Gandhi, *Luminescence* **2020**, *35*, 90.
[11] D. Q. Zhang, C. Ribelayga, S. C. Mangel, D. G. McMahon, *J. Neurophysiol.* **2002**, *88*, 1245.
[12] K. Hanaoka, K. Kikuchi, H. Kojima, Y. Urano, T. Nagano, *J. Am. Chem. Soc.* **2004**, *126*, 12470.
[13] A. Voegelin, S. Pfister, A. C. Scheinost, M. A. Marcus, R. Kretzschmar, *Environ. Sci. Technol.* **2005**, *39*, 6616.
[14] S. V. Eliseeva, I. P. Golovach, V. S. Liasotskyi, V. P. Antonovich, S. Petoud, S. B. Meshkova, *J. Lumin.* **2016**, *171*, 191.
[15] Y. Liu, Q. L. Shi, J. L. Yuan, *Chin. Chem. Lett.* **2015**, *26*, 1485.
[16] O. Reany, T. Gunnlaugsson, D. Parker, *Chem. Commun.* **2000**(6), 473.
[17] M. L. Aulsebrook, B. Graham, M. R. Grace, K. L. Tuck, *Tetrahedron* **2014**, *70*, 4367.
[18] P. Carol, S. Sreejith, A. Ajayaghosh, *Chem. – An Asian J.* **2007**, *2*, 338.
[19] N. C. Lim, H. C. Freake, C. Brückner, Chem. A Eur. J. **2005**, *11*, 38.
[20] S. Khullar, S. Singh, P. Das, S. K. Mandal, *ACS Omega* **2019**, *4*, 5283.
[21] M. R. Winnett, P. Mini, M. R. Grace, K. L. Tuck, *Inorg. Chem.* **2020**, *59*, 118.
[22] M. L. Aulsebrook, M. Starck, M. R. Grace, B. Graham, P. Thordarson, R. Pal, K. L. Tuck, *Inorg. Chem.* **2019**, *58*, 495.
[23] M. L. Aulsebrook, S. Biswas, F. M. Leaver, M. R. Grace, B. Graham, A. M. Barrios, K. L. Tuck, *Chem. Commun.* **2017**, *53*, 4911.
[24] R. A. Poole, F. Kielar, S. L. Richardson, P. A. Stenson, D. Parker, *Chem. Commun.* **2006**(39), 4084.
[25] X. Wang, X. Wang, Y. Wang, Z. Guo, *Chem. Commun.* **2011**, *47*, 8127.
[26] C. Welch, S. J. Archibald, R. W. Boyle, *Synthesis (Stuttg)* **2009**, *2009* (4), 551.
[27] E. Toth, E. Brucher, I. Lazar, I. Toth, *Inorg. Chem.* **1994**, *33*, 4070.
[28] M. C. Heffern, L. M. Matosziuk, T. J. Meade, *Chem. Rev.* **2014**, *114*, 4496.
[29] A. S. Kristoffersen, S. R. Erga, B. Hamre, Ø. Frette, *J. Fluoresc.* **2014**, *24*, 1015.
[30] F. S. Richardson, *Chem. Rev.* **1982**, *82*, 541.
[31] A. A. Boali, M. Mansha, A. Waheed, N. Ullah, *J. Taiwan Inst. Chem. Eng.* **2018**, *91*, 420.
[32] S. Wen, G. Zhang, R. Zhang, L. Zhang, L. Liu, *RSC Adv.* **2017**, *7*, 19808.
[33] X. Song, Y. Ma, X. Ge, H. Zhou, G. Wang, H. Zhang, X. Tang, Y. Zhang, *RSC Adv.* **2017**, *7*, 8661.
[34] F. Weigend, *Phys. Chem. Chem. Phys.* **2006**, *8*, 1057.
[35] A. Suwattanamala, D. Appelhans, M. Wenzel, K. Gloe, A. L. Magalhães, J. A. N. F. Gomes, *Chem. Phys.* **2006**, *320*, 193.

SUPPORTING INFORMATION

Additional supporting information may be found online in the Supporting Information section at the end of this article.

How to cite this article: Waheed A, Abdel-Azeim S, Ullah N, Oladepo SA. Design and synthesis of two new terbium and europium complex-based luminescent probes for the selective detection of zinc ions. *Luminescence*. 2020;1–10. https://doi.org/10.1002/bio.3883